Characterization of Reflected Shock Tunnel Air Conditions using a Simple Method

Sangdi Gu (顾桑迪)[1,2,a], Herbert Olivier[1], Chih-Yung Wen (温志湧)[2], Jiaao Hao (郝佳傲)[2], and Qiu Wang (汪球)[3]

[1]Shock Wave Laboratory, RWTH Aachen University, Templergraben 55, 52062 Aachen, Germany.
[2]Department of Aeronautical and Aviation Engineering, The Hong Kong Polytechnic University, Kowloon, Hong Kong, China.
[3]State Key Laboratory of High Temperature Gas Dynamics, Institute of Mechanics, Chinese Academy of Sciences, No. 15 Beisihuanxi Road, Beijing, 100190, China.

Abstract

A new method to characterize air test conditions in hypersonic impulse facilities is introduced. It is a hybrid experimental-computational rebuilding method which uses the Fay-Riddell correlation with corrections based on thermochemical nonequilibrium computational fluid dynamic results. Its benefits include simplicity and time-resolution, and, using this method, a unique characterization can be made for each individual experimental run. Simplicity is achieved by avoiding the use of any optical techniques and overly expensive numerical computations while still maintaining accuracy. Without making any assumptions to relate the reservoir conditions to the nozzle exit conditions, the work done characterizing four test conditions in a reflected shock tunnel is presented. In this type of facility, shock compression is used to produce an appropriate reservoir which is then expanded through a nozzle to produce hypersonic flow. Particular focus is given to the nozzle exit total enthalpy where a comparison is made with the reservoir enthalpy obtained using the measured shock speed and pressure in the shock tube. Good agreement is observed in all cases providing validation of the new approach. Additionally, static pressure measurements showed clearly that conditions III and IV have a thermochemical state which likely froze shortly after the nozzle throat. Also, the nozzle flow is shown to be almost isentropic. Due to the simplicity of the current method, it can be easily implemented in existing facilities to provide an additional independent estimate alongside existing results.

1 Introduction

The reflected shock tunnel is a vital tool used in experimental hypersonics to facilitate research on all areas of current interest in high-speed flows, including boundary layer transition, shock-boundary layer interaction, thermochemical nonequilibrium, and hypersonic propulsion. The TH2 reflected shock tunnel (located at RWTH Aachen University in Aachen, Germany) is shown in Figure 1; it will be the focus of this paper. The TH2 is driven

---

[a]Corresponding author. Email: sangdi.gu@polyu.edu.hk

by a 6 m long helium driver connected to a 15.4 m long shock tube, with both sections having the same inner diameter of 140 mm. The nozzle is a 5.8º half angle conical nozzle with a throat diameter of 37 mm and an exit diameter of 586 mm, resulting in a geometric area ratio of 250. For all the conditions, the shock tube is initially filled with air at room temperature consisting of 0.79 N_2 and 0.21 O_2 by mole fraction. The nozzle and dump tank are initially evacuated to a pressure of around 20 Pa prior to the shot. Two pressure transducers are installed, 1.247 m apart, near the downstream end of the shock tube for pressure and shock speed measurements. Further details on TH2 is given in Ref. [1].
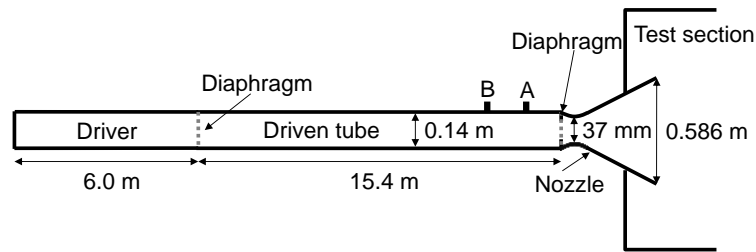

Figure 1. The TH2 reflected shock tunnel with a conventional driver. Pressure transducers A and B are located 0.106 m and 1.353 m from the downstream end of the shock tube respectively. Not to scale.

The TH2 operates as a conventional reflected shock tunnel. Upon rupture of the diaphragm separating the driver section and the driven section, the high-pressure helium driver gas generates a propagating normal shock in the driven tube filled with the test gas. The generated shock wave propagates towards the nozzle and reflects at the end of the driven tube which stagnates the test gas and creates a reservoir of high temperature and high-pressure test gas. The diaphragm at the nozzle inlet then ruptures and this allows the reservoir of test gas to expand through a converging-diverging nozzle producing the hypersonic test condition.

As discussed in Ref. [2, 3], an important challenge on the operation of reflected shock tunnels (and hypersonic impulse facilities in general) is the characterization of the generated test conditions. This is important due to its impact on the interpretation of the experimental results. However, this is a non-trivial task because, generally, only a limited amount of freestream flow property data can be measured at the nozzle exit. The exception may be if an advanced optical technique such as tuneable diode laser absorption spectroscopy [4] or coherent anti-stokes Raman spectroscopy [5] is used, but these techniques are complex, difficult to set up and generally cannot be done simultaneously with the experiments, which means an individual freestream estimate for each shot cannot be obtained. Full-facility time-accurate Navier-Stokes simulations are sometimes used to characterize these test conditions [6-8]; however, an obvious disadvantage is that an individual calibration for each run is impractical due to the computational time required. This is unless a perfectly steady flow is assumed

and only the nozzle flow is simulated to ease the computational burden [9, 10], in which case the result would not be time-resolved. Likewise, if a quasi-one-dimensional flow is assumed instead [11], accuracy will be sacrificed.

In this paper, a simple yet accurate hybrid experimental-computational approach is presented which allows for the determination of time-resolved estimates of test conditions for each individual run via small pressure and heat flux probes which can be used simultaneously with any on-going experiments without interference. The method uses the Fay-Riddell correlation with corrections based on thermochemical nonequilibrium computational fluid dynamic (CFD) results for small spheres which are rigorously assessed and validated. Simplicity is achieved by avoiding the use of any optical techniques and overly expensive numerical computations. Using this method, the work done characterizing four nominal test conditions in the TH2 reflected shock tunnel is presented along with the uncertainties. Particular focus is given to the nozzle exit total enthalpy where a comparison is made with the reservoir enthalpy obtained using the measured shock speed and pressure in the shock tube. While it is commonly assumed that the reservoir enthalpy is equal to the nozzle exit total enthalpy, this assumption is not made in the current work to preserve generality. Also examined is the existence of isentropic nozzle flows.

2 Methodology

The aforementioned hybrid experimental-computational approach is based on the experimental rebuilding technique of Ref. [12]. It involves deducing the test condition from simultaneous pitot pressure, static pressure and stagnation point heat flux measurements at the nozzle exit; the procedure is illustrated in Figure 2. Firstly, the total enthalpy of the test condition is determined by relating the measured static pressure, pitot pressure and stagnation point heat flux to the total enthalpy through the thermochemical equilibrium Fay-Riddell correlation for spheres. The correlation was obtained by curve fitting the results from a large number of numerical solutions of the self-similar boundary layer equations for a range of conditions (freestream static pressure $= 450 - 37600$ Pa, freestream velocity $= 1.77 - 7.00$ km/s, and wall temperature $= 300 - 3000$ K) while assuming thermochemical equilibrium, and constant Prandtl number and Lewis number through the boundary layer [13]. From Ref. [13], the correlation is given as

$$q_w = K\left(0.76 Pr^{-0.6}(\rho_e \mu_e)^{0.4}(\rho_w \mu_w)^{0.1}\sqrt{\left(\frac{du_e}{dx}\right)_s}(h_{0e} - h_w) * \left[1 + (Le^{0.52} - 1)\left(\frac{h_D}{h_{0e}}\right)\right]\right) \tag{1}$$

where q, ρ, μ, u, h, Pr and Le denote the heat flux, density, dynamic viscosity, velocity, specific enthalpy, Prandtl number and Lewis number respectively, while subscript 0 denote total conditions and subscripts e and w denote the condition at the boundary layer edge on the stagnation streamline and condition at the wall respectively.
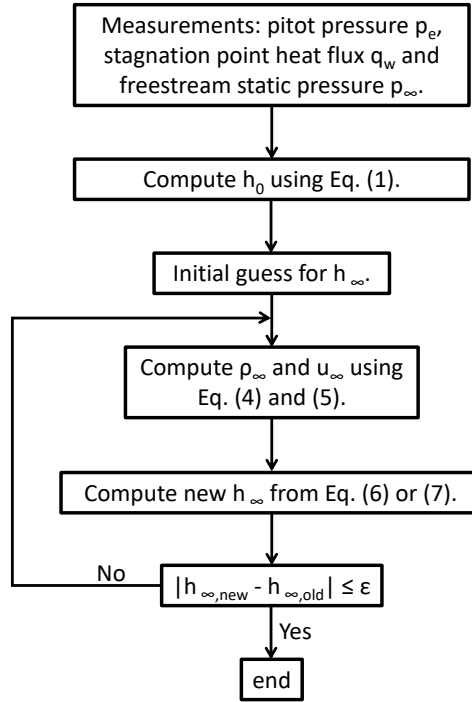
Figure 2. Flowchart of Olivier's [12] freestream rebuilding method.

The constant K is a correction factor whose value depends on the test condition, and it is defined as

$$K = \frac{q_{CFD,NONEQ}}{q_{FR}}$$

where $q_{CFD,NONEQ}$ and q_{FR} denote the stagnation point heat flux calculated from thermochemical nonequilibrium CFD simulations and the Fay-Riddell correlation respectively. This is not in the original Fay-Riddell correlation but is added here in the rebuilding method to account for the deviation of the correlation from the more accurate CFD results, which can be as much as 30 % for certain conditions as shown by Ref. [14]. Based on its formulation as mentioned earlier, the deviation may be contributed by nonsimilar boundary-layer profiles, varying Prandtl number and Lewis number through the boundary layer, thermochemical nonequilibrium, and even the quality of the curve fit. In the current work, the value of K in equation 1 is determined from two-temperature nonequilibrium Navier-Stokes simulations for each nominal test condition and this is discussed in detail in the next section. As will be shown later, the value of K is not particularly sensitive to the freestream which means that one can simply just use a rough estimate of the freestream of a nominal test condition to determine the correct value of K which will then remain as a constant of that test condition.

The derivative $(du/dx)_s$ is the tangential velocity gradient at the edge of the boundary layer, which, according to the Newtonian flow model [13], can be calculated using

$$\left(\frac{du_e}{dx}\right)_s = \frac{1}{R_N}\sqrt{\frac{2(p_e - p_\infty)}{\rho_e}} \tag{2}$$

where R_N and p is the sphere radius and gas pressure respectively. Inaccuracies in the determination of $(du/dx)_s$ (that is, deviation of the tangential velocity gradient between the Newtonian theory and the more exact CFD value) would also inevitability contribute to errors when applying the Fay-Riddell correlation, and this is discussed in detail in the next section.

The variable h_D is termed by Fay and Riddell [13] as the dissociation enthalpy at the boundary layer edge on the stagnation streamline which they defined as,

$$h_D = \sum_{atoms} c_{i,e}(\Delta h_f)^\circ{}_i \tag{3}$$

where c_i is the mass fraction of species i, $(\Delta h_f)^\circ{}_i$ is the heat of formation of species i at 0° K per unit mass and the summation extends over atomic oxygen and nitrogen only.

With the right correction factors, one can theoretically use any stagnation point heat transfer correlation (there exists numerous correlations [13, 14]) in the current rebuilding method [15]. Equation 1 is used here because it is one of the most well-known and commonly used correlation in the community. Also, as shown in Ref. [12, 16], this correlation works reasonably in the rebuilding method even without the correction factor K, that is, this correlation does not require large corrections (K is close to 1) and this will be shown in the next section.

The spherical heat flux probe should be no larger than 20 mm in diameter to avoid heat flux augmentation from the radiating flow contaminants in shock tunnels [17, 18]. Radiative heating increases with increasing body size while convective heating decreases with increasing body size [14]. Hence, by using a small heat flux probe, dominance by convective heating is forced, which is desired here. In the current work, 20 mm diameter spheres are used as probes for measuring the pitot pressure and stagnation point heat flux. The static pressure is measured using the slender static pressure probe described, tested, and validated in Ref. [19].

Once the total enthalpy is determined, an iterative process is carried out to deduce the other flow properties. Using the conservation equations across a normal shock wave (Rankine-Hugoniot jump conditions), Olivier [12] derived the following relations for the stagnation streamline:

$$\rho_\infty u_\infty = \rho_e \sqrt{2(h_0 - h_\infty)}\left(1 - \sqrt{1 - \frac{1}{\rho_e}\frac{p_e - p_\infty}{h_0 - h_\infty}}\right) \tag{4}$$

and

$$\rho_\infty u_\infty^2 = 2\rho_e(h_0 - h_\infty)\left(1 - \sqrt{1 - \frac{1}{\rho_e}\frac{p_e - p_\infty}{h_0 - h_\infty}}\right)$$ (5)

where the subscript ∞ denotes the freestream conditions and the other notations are consistent with those for Eq. (1). These two equations are valid for a wide range of conditions, including very high enthalpy conditions, and for equilibrium and nonequilibrium [12]. The freestream enthalpy, h_∞, is related by,

$$h_\infty = f(p_\infty, \rho_\infty)$$ (6)

for thermochemical equilibrium, and

$$h_\infty = \frac{5}{2}R_{froz}T_\infty + h_{froz} + \sum_{molecules} c_{i,froz}(R_i T_\infty)$$ (7)

for frozen flow [20], where R_{froz} is the specific gas constant of the frozen gas mixture, R_i is the specific gas constant of molecular species i with mass fraction c_i in the frozen mixture and h_{froz} consists of the frozen vibrational, electronic and chemical enthalpy of the gas mixture. Hence, it is possible to iteratively determine the freestream density ρ_∞, temperature T_∞ and velocity u_∞ using the said equations, along with the deduced total enthalpy, h_0, and the measured static pressure, p_∞. Unless otherwise stated, all equilibrium calculations described in this work are made using Cantera [21].

3   The Fay-Riddell correction factors

3.1   CFD simulations

To determine K in equation 1, two-temperature thermochemical nonequilibrium CFD simulations of axisymmetric flow around a 20 mm diameter sphere, using the Eilmer3 code from The University of Queensland, is conducted for four test conditions. As shown in Ref. [22], Eilmer3 is a validated and established tool for the simulation of various high enthalpy flows in thermochemical nonequilibrium. Accurate predictions of the wall heat flux in such flows are demonstrated in Ref. [23, 24] by comparing to experimental measurements. Due to the reliability of the code, it has been used as a validation tool to validate new models for high-enthalpy blunt body viscous flows as shown in Ref. [25, 26].

Eilmer3 is an open-source explicit Navier–Stokes solver for transient compressible flow in two and three dimensions based on the integral form of the Navier-Stokes equations. The core gas dynamics formulation is based on finite-volume cells. The inviscid fluxes are calculated at the cell interfaces using an adaptive flux calculator in which the equilibrium flux method [27] is applied near shocks and the AUSMDV scheme [28] is applied elsewhere. The viscous fluxes are calculated using the averaged values of the viscous stresses at the cell

vertices. A modified van Albada limiter [29] and a Monotonic Upstream-centred Scheme for Conservation Laws [30] reconstruction scheme are used to obtain second-order spatial accuracy. The time advancement procedure is based on the operator-splitting method [31] and the time integration uses the predictor-corrector method. The thermochemical effects are handled with specialised updating schemes that are coupled into the overall time-stepping scheme. Numerical stability is maintained by the Courant–Friedrichs–Lewy (CFL) criterion, with a CFL value of 0.9 used in the current work. The species mass diffusion is modelled using the multicomponent diffusion model of Ramshaw and Chang [32] where each species has a separate diffusion coefficient that contributes to the overall diffusion. The heat flux for thermochemical nonequilibrium flows is calculated via the formulation given by Ref. [33]. The reader is referred to Ref. [22, 34] for further details on Eilmer3, including its formulation and validation. The current work makes use of the existing features of the code without any further development.

Table 1. Inflow conditions used in the CFD simulations. The chemical composition is 0.79 N_2 and 0.21 O_2 by mole fraction.

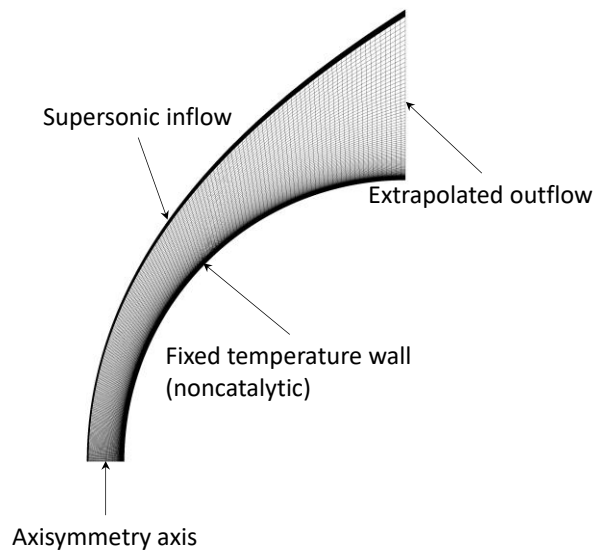| TH2 Condition	p_∞, Pa	T_∞, K	u_∞, m/s
I	520	100	1650
II	2000	225	2250
III	2500	250	2600
IV	7300	700	3400

Figure 3. The computational domain, boundary conditions, and mesh.

The CFD inflow conditions are shown in Table 1 which are the nominal estimates of four TH2 test conditions. These values are representative averages of a series of shots (up to 11 repeats of each condition) performed in the experimental campaign of 2018-2020, with the values of each particular shot determined using the original rebuilding method of Olivier [12] assuming thermochemical equilibrium. As will be shown later, the

7

value of K is not particularly sensitive to the freestream which means that one can simply just use a rough estimate of the freestream of a nominal test condition to determine the correct value of K.

The thermochemical nonequilibrium air model (two-temperature model) of Park [35] is used for the simulations. To account for the vibration-dissociation coupling, the dissociation/recombination reactions are controlled by an effective temperature, T_c, given as $T_c=T_{tr}^{0.5}T_v^{0.5}$ where T_{tr} is the translational-rotational temperature and T_v is the vibrational temperature. The computational domain and the boundary conditions used for the current work is shown in Figure 3. The inflow boundary is made to be adaptive and fit with the shock front. A structured grid of 240 x 240 is used, subdivided into 240 blocks. Strong clustering is implemented at the shock front and normal to the wall, as shown in Figure 3. The clustering at the shock front is regular with a spacing of around 1.0 µm, while the clustering normal to the wall decreases in the radial direction with a minimum cell spacing of around 0.01 – 0.1 µm, depending on the condition, at the first cell from the wall at the stagnation point. Clustering is also made in the wall-tangential direction towards the axisymmetry axis in the current work, as shown in Figure 3. The minimum spacing in the tangential direction, which is found on the first cell from the axisymmetry axis, is around 10 µm. The average spacing in the wall-normal and wall-tangential directions is around 15 µm and 85 µm, respectively.

For predicting the surface heat flux, various computational scientists have stated that the wall cell Reynolds number needs to be below a certain value. Some authors state that any Re_{wall} value below 3 would give good results [36], while other authors state that the Re_{wall} value should be around 1 [37]. The later condition is achieved for the current work for all the simulated cases. An alternative mesh size criterion is given by Ref. [38] as $\Delta x \ll L_p$ where the characteristic length scale L_p is defined as

$$L_p = \frac{T_{wall}}{\left(\frac{dT}{dx}\right)_{wall}} \tag{8}$$

for the current case. This criterion is also achieved in the current work with Δx being about two orders of magnitude smaller than L_p.

3.2 Mesh independence study

A mesh independence study is carried out by testing with scaled meshes and comparing the heat flux distribution around the sphere. This is done for each test case. An example is shown in Figure 4 (a) for the nonequilibrium simulation of the TH2 condition I. The result is mesh independent when more than 180 x 180 cells are used. The same observation is made for the other test cases. Looking at Figure 4 (b), a distinct feature of a converged simulation is that the gradient of the heat flux versus angle curve is about 0 at the stagnation point

and the heat flux distribution follows a smooth cosine-like curve. These features are indeed consistent with what we expect from the heat flux distribution around a sphere according to Murzinov's result [39],

$$\frac{q_w}{(q_w)_0} = 0.55 + 0.45\cos(2\theta) \tag{9}$$

and Lees' theory [40],

$$\frac{q_w}{(q_w)_0} = \frac{\frac{1}{2}\theta\sin\theta\left(\cos^2\theta + \left(\frac{1}{\gamma_\infty M_\infty^2}\right)\sin^2\theta\right)}{\left[\int_0^\theta \theta\sin^2\theta\left(\cos^2\theta + \left(\frac{1}{\gamma_\infty M_\infty^2}\right)\sin^2\theta\right)d\theta\right]^{\frac{1}{2}}} \tag{10}$$

with $(q_w)_0$, θ, γ_∞ and M_∞ denoting the stagnation point heat flux, angle from stagnation point, freestream heat capacity ratio and freestream Mach number respectively. The current converged results agree particularly well with Murzinov's result as shown in Figure 4 (b) with the results being indistinguishable from one another. This may be because Murizinov's equation was derived via solutions of the exact boundary-layer equations while Lees' equation was obtained using the local similarity method and, thus, the former is more consistent with the current Navier-Stokes solutions.
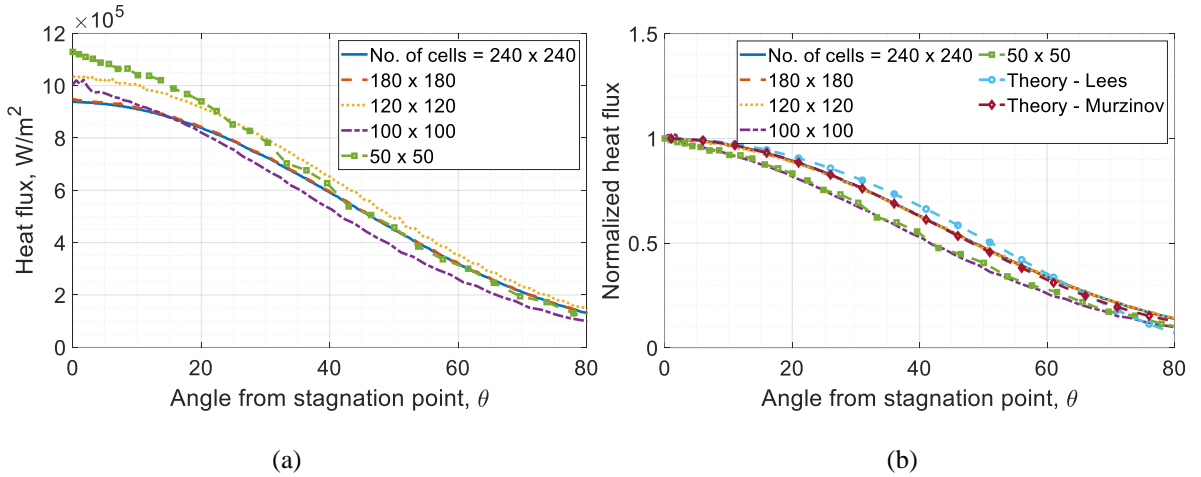

(a)   (b)

Figure 4. Simulated nonequilibrium (a) absolute and (b) normalized heat flux distributions around a 20 mm diameter sphere for the TH2 condition I.

Between the 100 x 100 case and 120 x 120 case, the strength of the clustering is increased in the shock layer, wall-normal direction, and wall-tangential direction. This immediately resulted in the final normalized heat flux distribution without the absolute heat flux being converged. This also explains the slight increase in the stagnation point heat flux from 100 x 100 to 120 x 120 when the overall trend is decreasing with increasing number of cells, reflecting the complexity and non-linearity of the solution of the stagnation point heat flux which is influenced by many aspects of the flowfield.

Using the results from the 240 x 240, 180 x 180, and 120 x 120 cases, Richardson extrapolation [41] is employed to extrapolate the asymptotic zero grid spacing values of the stagnation point heat flux. The result for the TH2 condition I is shown in Figure 5. The zero grid spacing value differs from that obtained in the finest resolution case (240 x 240) by less than 0.3 %. Similar observations are made for the other conditions. This further demonstrates the convergence of the current results. From Ref. [41], through calculation of the Grid Convergence Index (GCI), the numerical uncertainties of the current results are estimated to be less than 0.5 % which, for all intent and purposes of the current work, can be considered negligible.
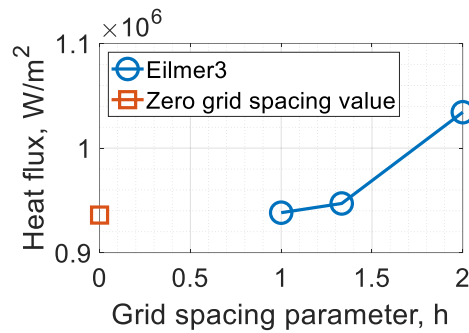

Figure 5. Stagnation point heat flux at zero grid spacing as calculated using Richardson extrapolation on converging grids for the TH2 condition I.

3.3   Results

The CFD simulation results, $q_{CFD,NONEQ}$, are summarized in Table 2 along with the Fay-Riddell predictions, q_{FR}, and the Fay-Riddell correction factor, K. For consistency, all the q_{FR} values in the table are calculated using Pr = 0.7, Le = 1.4, Sutherland's law for the viscosity, and Newtonian flow model for the tangential velocity gradient. For the four TH2 conditions, the Fay-Riddell correlation underpredicts the heat flux by about 10 - 20 %. The correction factor does not vary significantly between the four conditions, and it varied hardly at all between the first three conditions. This shows that the correction factor is not particularly sensitive to the condition which means that the same value of the correction factor can be used for a given test condition without having to iterate every time a new freestream estimate is obtained. Nevertheless, this is not to say that the Fay-Riddell correlation always underpredicts the heat flux by about 10 - 20 % for any condition. The same study is carried out for the HEK-X condition ($p_\infty = 116$ kPa, $u_\infty = 7.00$ km/s and $T_\infty = 4600$ K) of Ref. [42], which is a very different condition to any of the TH2 conditions. In this case, the Fay-Riddell correlation overpredicted the heat flux by 30 % (resulting in K = 0.7). Therefore, it is still necessary to obtain a correction factor for each nominal test condition.

As the Fay-Riddell correlation, equation 1, was derived to predict the equilibrium stagnation point heat flux, one would expect the deviation of the Fay-Riddell prediction with the nonequilibrium CFD prediction to increase with decreasing freestream density as the flow tends towards the frozen limit, given the sphere size is kept

constant. One might also think that the deviation would maybe increase with increasing freestream velocity as this increases the frozen and equilibrium bounds thus creating a possibility for larger deviations. However, these statements assume that the value of the tangential velocity gradient one uses in the Fay-Riddell correlation is always correct. In reality, this is not the case as the Newtonian flow model is used for determining the tangential velocity gradient, which is not particularly accurate. It is unclear how the accuracy of the Newtonian flow model varies with flow condition; no systematic investigation of this is reported in literature. So, the deviation of equation 1 with nonequilibrium CFD results does not follow some trivial pattern, and this has already been shown by Ref. [14] who performed several hundred nonequilibrium CFD simulations for spheres of different sizes under a wide range of freestream conditions. In particular, their results showed that the deviation has no correlation with the total enthalpy. As a corollary, one can find fortuitous agreements between the equilibrium Fay-Riddell correlation and nonequilibrium CFD results due to incorrect tangential velocity gradients predicted from the Newtonian flow model leading to cancellation of errors. To support the current discussion, identification of the influencing parameters via an Uncertainty Quantification approach should be made in the future.

Table 2. Summary of results from the nonequilibrium simulations of the sphere showing the predicted stagnation point heat flux from CFD, $q_{CFD,NONEQ}$, and the Fay-Riddell correlation, q_{FR}.

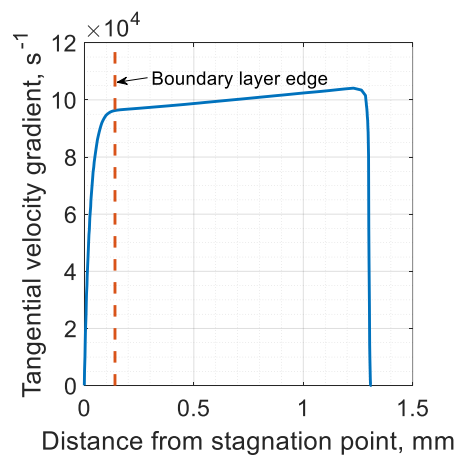| Condition	I	II	III	IV
$q_{CFD,NONEQ}$, MW/m^2	0.94	3.75	6.3	16.2
q_{FR}, MW/m^2	0.82	3.22	5.5	14.5
FR correction factor, K	1.15	1.16	1.14	1.12

Figure 6. Tangential velocity gradient along the stagnation streamline for the TH2 condition I test case.

Subsequently, one can also find cases where the Fay-Riddell correlation fails to predict even the equilibrium stagnation point heat flux due to the use of inaccurate tangential velocity gradients. To illustrate this, thermochemical equilibrium CFD simulations are performed for the TH2 condition I and II using the same computational methodology described above. The stagnation point heat flux results are summarized in Table 3.

The variable $q_{CFD,EQ}$ refers to the stagnation point heat flux calculated from equilibrium CFD, while the variables $q_{FR,CFD}$, $q_{FR,Newtonian}$ and $q_{FR,Olivier}$ refer to the stagnation point heat flux calculated from the Fay-Riddell correlation using, respectively, the tangential velocity gradient from CFD, Newtonian theory (equation 2) and Olivier's equation [43],

$$\left(\frac{du_e}{dx}\right)_s = \frac{u_\infty}{R_N}\frac{1+\bar{\Delta}}{\bar{\Delta}}\frac{p_s-p_2}{\rho_\infty u_\infty^2}\frac{\rho_2}{\rho_s} \tag{11}$$

where $\bar{\Delta} = \Delta/R_N$ is the dimensionless shock stand-off distance which is obtained from CFD in the current study. The results show that errors up to 9 % is observed when equation 2 is used. Equation 11 gives a slightly more accurate prediction than equation 2, with the discrepancy being about 5 %. The best result is achieved when the tangential velocity gradient from CFD is used, as expected, obtaining agreement to within 3 %. A corollary of this result is that the Fay-Riddell correlation is accurate in estimating the equilibrium stagnation point heat flux for the current conditions given accurate values of the tangential velocity gradient. Regarding the extraction of the tangential velocity gradient from CFD, as Fay and Riddell [13] defined it in equation 1 to be that at the boundary layer edge, we need to define what is the boundary layer edge so that the gradient can be extracted at the correct location. In the current work, the edge of the boundary layer is defined as the location where the total enthalpy is 99 % of the freestream total enthalpy for consistency with Ref. [44, 45] who performed a similar analysis. Nevertheless, the tangential velocity gradient is not particularly sensitive to the location along the stagnation streamline, as shown in Figure 6 for the TH2 condition I for example, with its value varying by less than 10 % within the entire inviscid shock layer.

Table 3. Summary of results for the equilibrium simulations of the sphere. $q_{CFD,EQ}$ refers to the stagnation point heat flux calculated from equilibrium CFD, while $q_{FR,CFD}$, $q_{FR,Newtonian}$ and $q_{FR,Olivier}$ refer to the stagnation point heat flux calculated from the Fay-Riddell correlation using the velocity gradient from CFD, Newtonian theory and Olivier's equation respectively.

Condition	I		II	
	Value, MW/m²	Error, %	Value, MW/m²	Error, %
$q_{CFD,EQ}$	0.89	-	3.54	-
$q_{FR,CFD}$	0.87	2	3.42	3
$q_{FR,Newtonian}$	0.82	8	3.22	9
$q_{FR,Olivier}$	0.93	5	3.72	5

Also, when comparing the $q_{CFD,EQ}$ values in Table 3 to the corresponding (conditions I and II) $q_{CFD,NONEQ}$ values in Table 2, one can see appreciable differences between the equilibrium and nonequilibrium heat flux values even for these two low enthalpy conditions. As the temperature here is not high enough to cause chemical nonequilibrium, the differences between the equilibrium and nonequilibrium results are caused by the vibrational nonequilibrium in the flow, as shown in Figure 7 for condition I. From this figure, vibrational nonequilibrium is

present all along the stagnation streamline, which influences the temperature profile and the shock stand-off distance. A larger T_v gradient is observed at the wall in the nonequilibrium result which ultimately causes $q_{CFD,NONEQ} > q_{CFD,EQ}$ for this case.
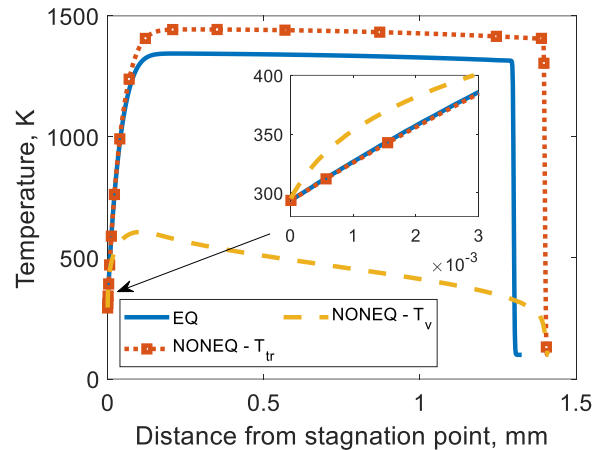

Figure 7. The temperature profiles along the stagnation streamline for the TH2 condition I.

Thus, by applying the correction factor, K, in the manner outlined in section 2, one effectively corrects for the shortcomings of the Fay-Riddell correlation which are contributed by circumstances including, but not limited to, the occurrence of thermochemical nonequilibrium and the calculation of the tangential velocity gradient. For using the correction factors in the rebuilding method, it is critical that they are obtained for the Newtonian model for the tangential velocity gradient as this is the model used in the rebuilding method.

3.4   On the potential uncertainties of the correction factors

In the preceding sections, much effort is devoted to ensure convergence of the numerical solutions of the Navier-Stokes equations with coupled thermochemical effects. It is assumed that the governing equations can correctly describe the physical phenomenon concerned in the current work (high enthalpy viscous flow around a sphere), thus, producing the absolute true stagnation point heat flux under given freestream conditions which is then used to correct the Fay-Riddell correlation. In this section, the validity of this assumption is discussed.

The limitations of the Navier-Stokes equations to model regions of large gradients, due to the break-down of the continuum assumption, were investigated by Ref. [38] and a Knudsen number, Kn, was defined using the local mean free path and the characteristic length scale of the flow property concerned, L_p (equation 8). For high Kn values (rarefied regime where Kn $\geq$ 1), there are not enough intensive particle collisions in such small length scales during a computational time step to justify a continuum description, and, thus, the limitations were demonstrated by modelling complex transient phenomenons with large gradients, namely shock-interface interaction, Richtmyer-Meshkov instability, and shock-bubble interaction. For the current test conditions for the

13

temperature gradients at the wall, $10^{-2} < Kn < 10^{-1}$ which lies in the transitional regime between the continuum ($Kn \leq 10^{-3}$) and rarefied regimes. This result, coupled with the fact that we are dealing with a steady-state flow problem rather than a transient flow problem, suggests the use of the Navier-Stokes equations without significant errors. Indeed, substantial work have been done on modelling high-enthalpy blunt body steady-state flows using the Navier-Stokes equations as reviewed by Ref. [46].
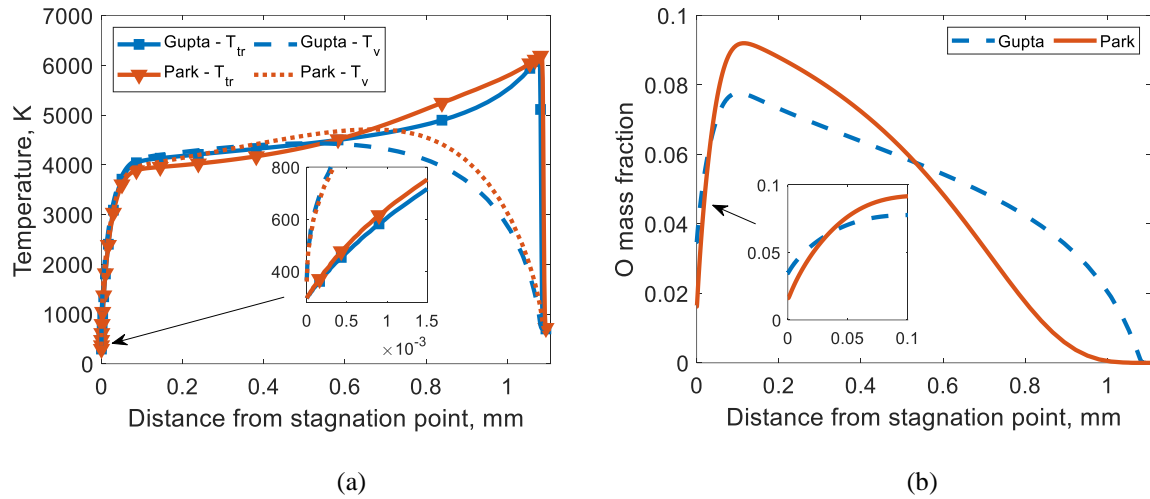

Figure 8. The (a) temperature and (b) O mass fraction profiles along the stagnation streamline for the TH2 condition IV.

Instead, a more significant source of uncertainty could be from the thermochemical nonequilibrium model used [47]. When using the two-temperature model, various parameters are available for tuning, including the chemical reaction rates and the vibrational-dissociation coupling. Since no particular configuration is widely regarded as the "best" or most accurate one, it is of interest to test different configurations and assess the influence on the stagnation point heat flux predictions. To address this, additional nonequilibrium simulations are carried out using the rates of Gupta [33] with $T_c = T_{tr}^1 T_v^0$, and the resulting $q_{CFD,NONEQ}$ values are compared with the ones in Table 2 which are obtained using the rates of Park [35] with $T_c = T_{tr}^{0.5} T_v^{0.5}$. Since these two configurations use the same vibrational-translational (VT) energy exchange rates, no differences in the stagnation point heat flux values are observed in the TH2 conditions I, II and III due to the absence of chemistry. On the other hand, due to the presence of O_2 dissociation in condition IV, a difference of 7 % is observed in $q_{CFD,NONEQ}$ between the Gupta and Park simulations with the values being 15.1 MW/m^2 and 16.2 MW/m^2 respectively.

With the diffusion component of the heat flux being almost negligible for this condition (less than 1% of the total heat flux), and the T_v gradient at the wall being similar among the two simulations as shown in Figure 8 (a), the observed difference in the heat flux is caused by the difference in the T_{tr} gradient at the wall as shown in the same figure. The difference in the T_{tr} gradient at the wall is the result of the different O_2/O chemical

14

nonequilibrium in the flow as shown in Figure 8 (b). The Park configuration predicts a greater O recombination in the boundary layer which leads to the higher T_{tr} gradient at the wall due to the heat release from this exothermic reaction.

Another potentially significant source of uncertainty is the surface catalycity. Similar to the discussion above on the configurations for the nonequilibrium modelling, the surface catalycity is relevant only if the temperature is high enough for molecular dissociation to occur. This corresponds to only condition IV in the current work. Since the current simulations for condition IV are conducted using a noncatalytic wall, any surface catalycity will serve to increase the stagnation point heat flux as demonstrated in Ref. [13, 46]. Though, the potential increase in the heat flux would be small for the Park simulation ($q_{CFD,NONEQ} = 16.2$ MW/m^2) because, as shown in Figure 8 (b), the atomic recombination is almost complete at the wall already without requiring any surface reactions. The potential increase in the heat flux would be larger for the Gupta simulation ($q_{CFD,NONEQ} = 15.1$ MW/m^2) because the atomic recombination is less complete at the wall, and it would drive the Gupta result closer to the Park result. The uncertainties caused by the nonequilibrium modelling and the surface catalycity are accounted for in the uncertainty analysis of the condition IV results in section 5.

Another aspect which requires consideration is regarding the thermochemical state of the freestream. Generally in reflected shock tunnels, the test gas is heated to a state with at least significant vibrational excitation, if not significant dissociation and ionization, before expanding to hypersonic conditions. The test gas should not be able to maintain thermochemical equilibrium during the rapid expansion process in most cases as simulated by Ref. [48] using the high-fidelity state-specific nonequilibrium model. Hence, one may ask: how much is the stagnation point heat flux influenced by the thermochemical state of the freestream given the total enthalpy remains fixed? Given the total enthalpy remains fixed, inspection of the Fay-Riddell correlation (equation 1) under thermochemical equilibrium shows that it can be reduced to a (weak) function of only the pitot pressure – $q_{FR} \approx f(p_{pitot}^{0.5})$ – with an exponent of 0.5. The pitot pressure is generally not very sensitive to the thermochemical state of the freestream, which is a well-known result since the 1960s [49]. Thus, the Fay-Riddell correlation is essentially "blind" to the thermochemical state of the freestream, which may be expected given this aspect was not considered in the study of Fay and Riddell [13].

Essentially, as described by Ref. [49], assuming a thermochemical equilibrium post-shock condition "tends to erase the nonequilibrium history of the nozzle expansion process". Hence, it is necessary to resort to thermochemical nonequilibrium Navier-Stokes simulations to answer the abovementioned question. Gökcen [45] presented an investigation of the question by comparing the nonequilibrium stagnation point heat flux computed

from two different freestreams with the same total enthalpy but different thermochemical states – one was in equilibrium while the other was frozen at a thermochemical state representative of a nozzle flow in a hypersonic facility. Gökcen showed that for lower total enthalpy conditions around 7 MJ/kg, the nonequilibrium stagnation point heat flux was uninfluenced by the thermochemical state of the freestream provided the total enthalpy was the same. This would be the case for the four TH2 conditions concerned in the current work where the total enthalpy is below 6 MJ/kg. This means that the rebuilding of the total enthalpy is independent of thermochemical state of the freestream and that the correction factors obtained in section 3 for an equilibrium freestream is also applicable if a frozen freestream is defined using equation 7 (since both $q_{CFD,NONEQ}$ and q_{FR} are uninfluenced by the freestream thermochemical state).

4   Determination of the Reservoir Enthalpy

A method is presented in section 2 to deduce the total enthalpy of a test condition based on pressure and heat flux measurements at the nozzle exit. It is of interest to compare this value to the corresponding reservoir enthalpy which can be determined from the measured shock speed and pressure in the shock tube. This comparison is conducted in the next section. Hence, the current section is dedicated to a detailed analysis on the method to determine the reservoir enthalpy.

In an ideal shock tube with a closed wall, for tailored interface conditions, the condition behind the reflected shock would be constant in time until the arrival of the reflected expansion wave. In this case, the reservoir enthalpy can be calculated using just the incident shock speed. However, in the real shock (driven) tube of a reflected shock tunnel, the reservoir condition changes with time. This is shown in Figure 9 for the reservoir pressure of the TH2 condition I at the transducer A (see Figure 1). Consequently, the method of determining the reservoir condition in real reflected shock tunnels involves anchoring the ideal reservoir pressure calculated from the measured incident shock speed to the measured reservoir pressure via an isentropic process. This is done in well-known shock tunnel condition estimating codes such as ESTC [50], STUBE [51], and STN [52]. To analyse the validity of this method, it is of interest to first investigate the cause of the varying reservoir condition in a real reflected shock tunnel.
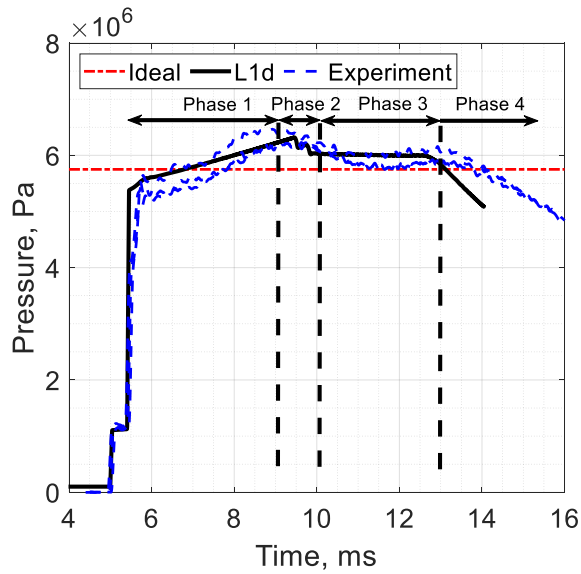
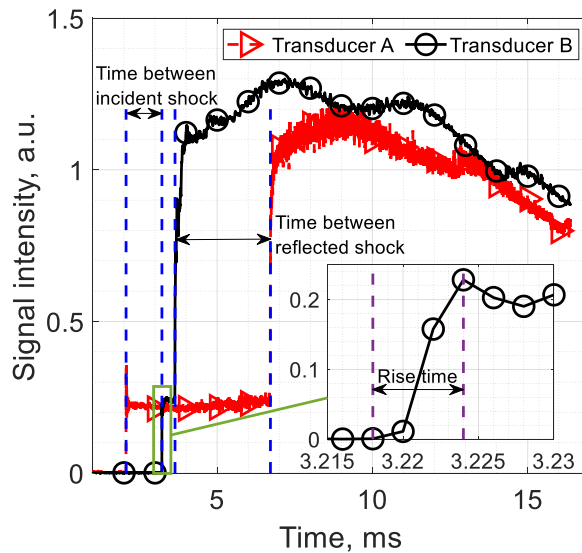**Figure 9. Nozzle reservoir pressure at transducer A for condition I.**

Figure 10. Raw experimental pressure transducer signals from the driven tube showing the shock arrival rise time and the time between shocks.

End-to-end modelling of the TH2 reflected shock tunnel is conducted using the L1d program from the University of Queensland [53]. L1d is a one-dimensional Lagrangian solver, which can model all the major processes within hypersonic impulse facilities, including reflected shock tunnels. These include flow area changes, pressure losses, diaphragm rupture, one-dimensional wave processes, wall shear-stress and heat transfer, contact-surface mixing, and high-temperature effects such as chemical dissociation and ionization. It is an explicit code which calculates the time evolution of internal flow processes in the facility. In the code, the facility is divided into gas slugs. The slugs are discretised, axially, into fixed-mass cells that move along the tube. As it is a one-dimensional code, this is no radial discretization. Boundary effects, such as heat transfer and wall friction, are

modelled at the wall boundary of each cell. The conservation equations for axial momentum and energy are applied to each cell. For each time step, the motion of the interface between gas cells is obtained by a Riemann solver [54] which, alongside the conservation equations, is used to solve for the flow properties. A look-up table for the thermochemical equilibrium properties of air, built using NASA's Chemical Equilibrium with Applications (CEA) [55], is used in L1d to simulate thermochemical equilibrium flows. The wall friction, wall heat transfer, and flow losses at sudden area changes are included in the gas-dynamic model using standard engineering correlations [56]. L1d has successfully simulated transient flow in numerous hypersonic impulse facilities including reflected shock tunnels [53, 57], expansion tunnels [58] and gun tunnels [59]. The current work makes use of the existing features of the code without any further development. Detailed description of the L1d code and its usage can be found in the aforementioned references.
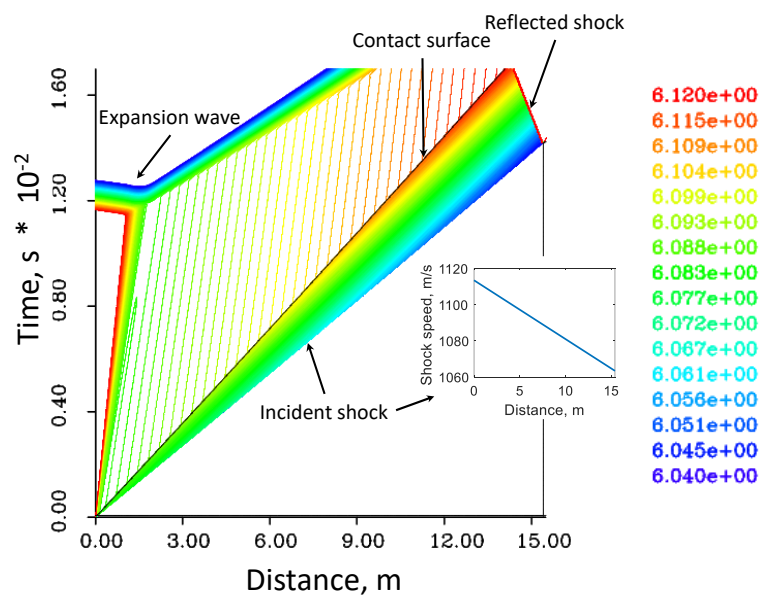

Figure 11. The x-t diagram and incident shock speed along the driven tube from the L1d simulation of the TH2 condition I.

For TH2, three gas slugs are considered: the driver gas slug, the test gas slug and the dump-tank gas slug (gas initially in the nozzle and dump-tank). As recommended by Ref. [57], one selects a coarse discretisation of the slugs for a trial simulation and then runs subsequent simulations with higher resolutions, increasing the number of cells by a factor of 1.5-2 each time. The resolution is increased until the shock speed and reservoir shock pressure converge to within 1 percent. The computed nozzle reservoir pressure at transducer A for the TH2 condition I is shown in Figure 9 along with the corresponding measurements from several different shots. According to Ref. [57], the uncertainty of the reservoir pressure measurement in a reflected shock tunnel can be around 3 %. From Figure 9, good agreement is observed between the measured and computed pressures. This is consistent with the good agreement in the incident shock speeds measured as the time-of-flight between two

18

pressure transducers (A and B in Figure 1), as shown in Figure 10, with L1d computing a shock speed of 1070 m/s compared to the measured shock speeds which is around 1060 m/s to 1080 m/s for the three shots shown in Figure 9. Even the reflected shock speed is in good agreement; 400 m/s from L1d compared to 390 m/s measured. The uncertainty of the shock speed measurement consists of a base level of uncertainty based upon the resolution of the data, and then also some uncertainty based on the rise time of the pressure measurement as shown in Figure 10. Thus, the actual time of arrival of the shock wave at the pressure transducer can be as early as the first point before the start of the rise time and as late as the first point after the end of the rise time. Based on this, the uncertainty of the incident shock speed measurement is around 1 % for the four TH2 conditions considered in the current work.
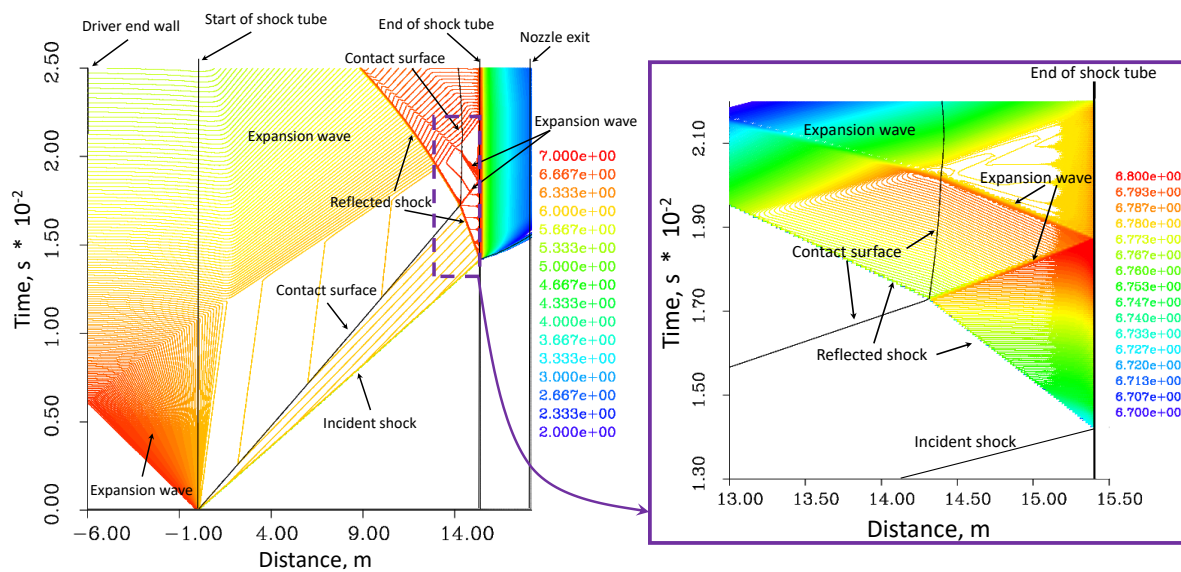

Figure 12. The x-t diagram of the TH2 condition I with the pressure contours in log10(p).

The different phases in Figure 9 are identified with the help of a x-t diagram with pressure contours as shown in Figure 11 and Figure 12. During phase 1, the pressure gradually increases. This gradual increase in pressure is due to the fact that the shock processed test gas slug has a higher pressure at its upstream end and a lower pressure at its downstream end, as shown in Figure 11. This is because of the deceleration of the shock speed through the shock tube, as shown in the same figure, due to the modelled viscous effects of wall friction and heat transfer. Test gas near the upstream end of the shock tube is shock processed to a higher pressure than the test gas near the downstream end of the shock tube because the shock speed is greater near the upstream end. Phase 2 marks the arrival of the expansion wave from the contact-surface after interaction with the reflected shock wave, as shown in Figure 12. This indicates that condition I is a slightly under-tailored condition. The flow is steadiest during phase 3 and, thus, should be used for experiments where temporal uniformity is important. Phase 4 marks the

arrival of the reflected expansion waves from the driver, as shown in Figure 12, effectively terminating the test time.

Comparing the above study to similar studies done on free-piston driven reflected shock tunnels (Stalker tunnels) [53, 57, 60], one sees that the transient behaviours of the reservoir state are characteristically different. This is because the piston face in a piston driven tunnel, which acts like the end wall of a conventional driver, is located very close ($\approx$ 1 m for the HEG condition III in Ref. [57]) to the upstream end of the driven tube after compressing the driver gas. As a result, waves originating from the piston face and waves reflecting off the piston face can catch the incident shock as shown in Ref. [57]. However, for a conventionally driven reflected shock tunnel with a long driver length, such as TH2 with a 6 m long driver, the reflected expansion waves from the driver end wall will chase but never catch the incident shock as shown in Figure 12.
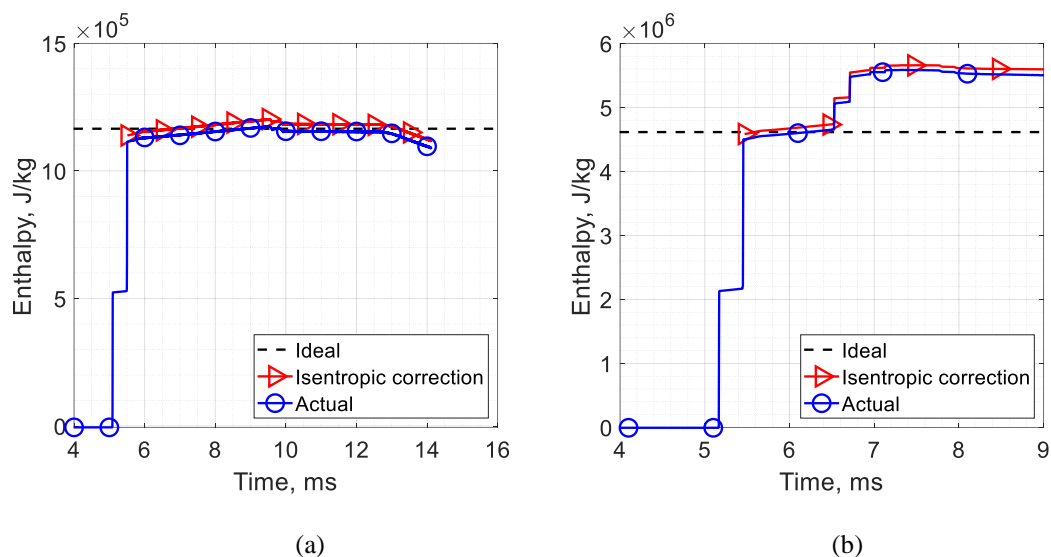

Figure 13. Reservoir enthalpy of the TH2 condition (a) I and (b) IV

Using the L1d results, it is useful now to conduct a numerical experiment to assess the validity of using the measured incident shock speed and reservoir pressure to determine the reservoir enthalpy via anchoring the ideal reservoir pressure to the measured reservoir pressure by an isentropic process. In the numerical experiment, this is carried out using the simulated shock speed between the TH2 transducers A and B and the simulated reservoir pressure at transducer A. The result is shown in Figure 13 (a) and agreement to within 2 % is observed with the simulated ('actual') reservoir enthalpy. Though for this condition, the reservoir enthalpy is quite constant despite variations being magnified by observing the reservoir pressure in Figure 9. Therefore, in this case, the actual reservoir enthalpy can be approximated well even using the constant ideal value without applying the isentropic correction on the reservoir pressure. The slight (within 2 %) over-prediction of the isentropic corrected result is due to the fact that the ideal reservoir enthalpy is about 2 % greater than the actual value at the point when the

ideal reservoir pressure matches the actual reservoir pressure. Therefore, a systematic error of this amount is formed when anchoring with the reservoir pressure.

As shown earlier, the TH2 condition I is a slightly under-tailored condition. It is now of interest to assess how the isentropic correction of the reservoir pressure performs for the TH2 condition IV which is an over-tailored condition. Compared to condition I, no expansion waves but two additional reflected shock waves can be observed in condition IV where the first reflected shock reflects off the contact surface before reflecting again at the end of the shock tube. The reservoir enthalpy is shown in Figure 13 (b). One can see that despite the existence of further shock processes, which is not exactly an isentropic process, the isentropic correction performs remarkably well in predicting the actual reservoir enthalpy to within 2 %. This is because there is little difference between shock compression and isentropic compression for relatively weaker shocks ($T_2/T_1 < 1.25$) [20]. This condition is indeed satisfied for condition IV, where the T_2/T_1 ratios from the two later reflected shocks are less than 1.1. Nevertheless, the temperature increase caused by these reflected shocks are still significant, therefore unlike for condition I, it is important to apply the isentropic correction because the reservoir enthalpy increases significantly from the ideal value calculated based on just one reflected shock.

5 Experimental results

5.1 Uncertainties

Before presenting the experimental results, it is necessary to summarize the methodology used to compute the uncertainties given to the results. In the subsequent sections, the uncertainties given to the results are computed according to the method described by Ref. [61] for a reflected shock tunnel where the uncertainty of a derived parameter is a function of the uncertainties of the various fundamental quantities (Gaussian error propagation). The uncertainties of the fundamental quantities considered in the current work are summarized in Table 4.

The driven tube fill pressure uncertainty is consistent with that given by Ref. [62] for another reflected shock tunnel. The driven tube fill temperature uncertainty is calculated assuming the laboratory varies from 291 K to 303 K. The shock speed uncertainty is obtained in this work as described in section 4. The reservoir pressure uncertainty is consistent with that quoted for the measurements presented in Figure 9. The pitot pressure uncertainty is that recommended by Ref. [61] for measurements in reflected shock tunnels. The stagnation point heat flux measurement, made using in-house coaxial thermocouples (type E), is assigned an uncertainty of 6 % based on Ref. [63]. The static pressure uncertainty is consistent with that given by Ref. [64] for a similar probe used in another hypersonic facility. While the possible sensitivity of the static pressure measurements to the

thermochemical effects has not been rigorously assessed, it may be deduced from existing numerical flat plate studies with u_∞ up to 6 km/s [65] that any sensitivity is likely negligible for the intent and purposes relevant to the current work. This is because any thermochemical effects in these very slender body flows are likely confined to the boundary layer with the inviscid flow remaining a calorically perfect gas since the shock wave from these bodies is very weak.

Table 4. **The uncertainties of the fundamental quantities considered in the current work**

	Driven tube fill pressure	Driven tube fill temperature	Shock speed	Reservoir pressure	Pitot pressure	Static pressure	Stagnation point heat flux	K for condition IV
Uncertainty, %	±0.3	±2	±1	±3	±3	±6	±6	±7
Ref.	[62]	This work	This work	[57]	[61]	[64]	[63]	This work

Regarding the uncertainties of the Fay-Riddell correction factors (K), the numerical uncertainty of the converged CFD solutions are negligible for the intent and purposes of the current work as discussed in section 3.2, while the errors originating from the physical models used are likely negligible for conditions I-III as discussed in section 3.4. Hence, the uncertainties of the correction factors are assumed to be zero for these conditions. However, for condition IV, a difference of 7 % in the stagnation point heat flux is observed when using two different thermochemical nonequilibrium models as shown in section 3.4. The correction factor of condition IV could inherit further uncertainty from the surface catalycity. Therefore, a conservative uncertainty of ±7 % is assigned to the correction factor of condition IV to account for the uncertainties in the nonequilibrium modelling and the surface catalycity.

Lastly, the uncertainty values assigned to the experimental reservoir enthalpies presented in the next section consists of an additional ±2 % on top of the uncertainty contributed by its fundamental quantities (driven tube fill conditions, shock speed, and reservoir pressure). This additional ±2 % uncertainty comes from the uncertainty of the method of determining the reservoir enthalpy as shown in the previous section.

5.2 The total enthalpy

Numerous runs of each nominal test condition are performed in the TH2 reflected shock tunnel. Typical results of the nozzle exit total enthalpy obtained from the rebuilding method is shown in Figure 14 for each condition. The corrected results are obtained using the correction factors in Table 2. Also shown is the corresponding reservoir enthalpy obtained from the measured shock speed and reservoir pressure for the same run. In reflected shock tunnels, the nozzle exit total enthalpy should be equal to or slightly lower than the reservoir

enthalpy. From Figure 14, for all cases, the uncorrected total enthalpy yields a physically unreasonable result as it is larger than the reservoir enthalpy even with the uncertainties considered. Good results are achieved after applying the correction factor as the total enthalpy is seen to match the reservoir enthalpy within the uncertainties. This further justifies the use of the correction factor and provides confidence in the predictions from the current rebuilding method.
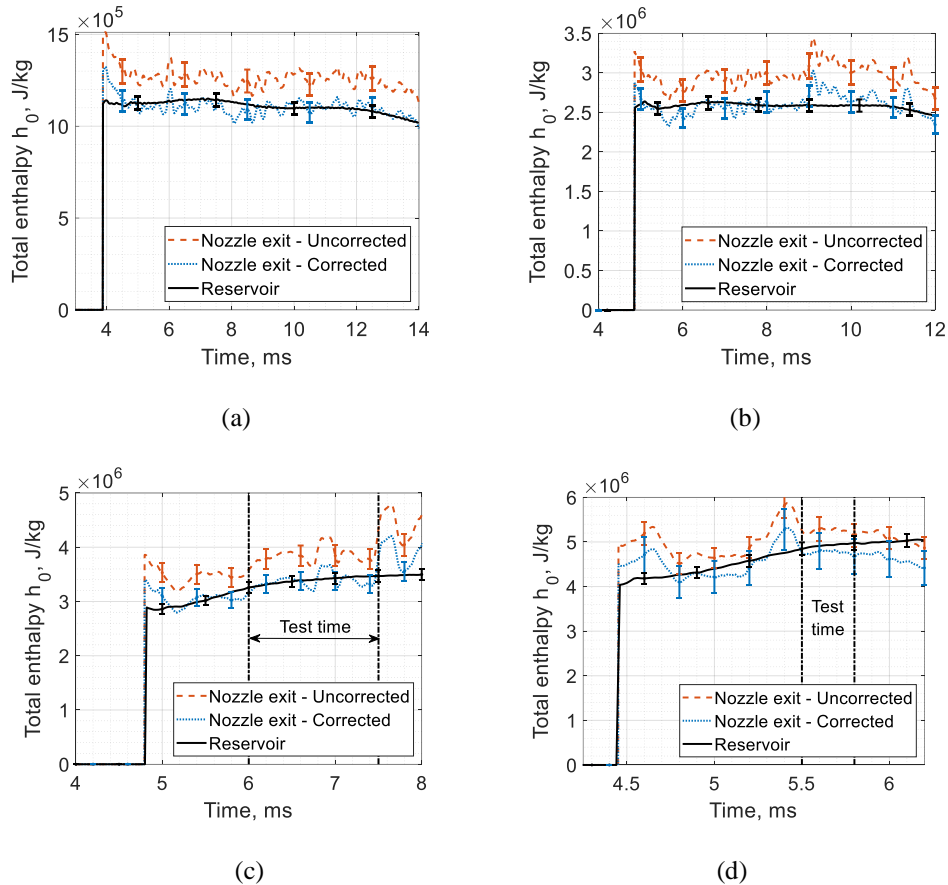

Figure 14. **The total enthalpy and reservoir enthalpy for the TH2 condition (a) I, (b) II, (c) III, and (d) IV.**

The good agreement between the reservoir enthalpy and the nozzle exit total enthalpy has a further implication. The accuracy of the method of determining the reservoir enthalpy using the measured shock speed and reservoir pressure as outlined in section 4 has been of significant interest [8]. This is assessed numerically in section 4 and the results indicated this method is accurate to within 2 % for the test conditions considered in the current work. So, the cross-validation of the experimental results shown in Figure 14 further suggests validation of the method for determining the reservoir enthalpy based on the measured shock speed and reservoir pressure.

Further interpreting the good agreement between the reservoir enthalpy and the nozzle exit total enthalpy, this result suggests no significant losses occur for the considered TH2 conditions in the reservoir and nozzle flow. Significant losses (reportedly due to radiation) have been reported by Ref. [66] for a pure argon flow for total

enthalpies above 10 MJ/kg. However, for the relatively low enthalpy air conditions considered in the current work, the obtained result of no detectable losses is unsurprising. Indeed, this result is commonly assumed when one characterizes the test conditions via Navier-Stokes simulations of the nozzle.

5.3   Other flow properties

Once the total enthalpy is determined, the other nozzle exit (freestream) flow properties can be determined according to the procedure outline in section 2. Examples of corrected and uncorrected results are shown in Figure 15 for condition I for an equilibrium freestream. Differences of up to 10 % is seen between the corrected and uncorrected results for the freestream velocity, temperature and density. The same is seen for the case of a frozen freestream and for the other TH2 conditions. The step rise seen at the beginning of all the traces is not physical and it exists simply because the freestream rebuilding code is programmed to start at some time during flow establishment and before the start of the test time. In reality, the rise in flow properties due to the flow arrival is more gradual as shown in Figure 17 for the freestream static pressure. This also holds for the total enthalpy shown in Figure 14.
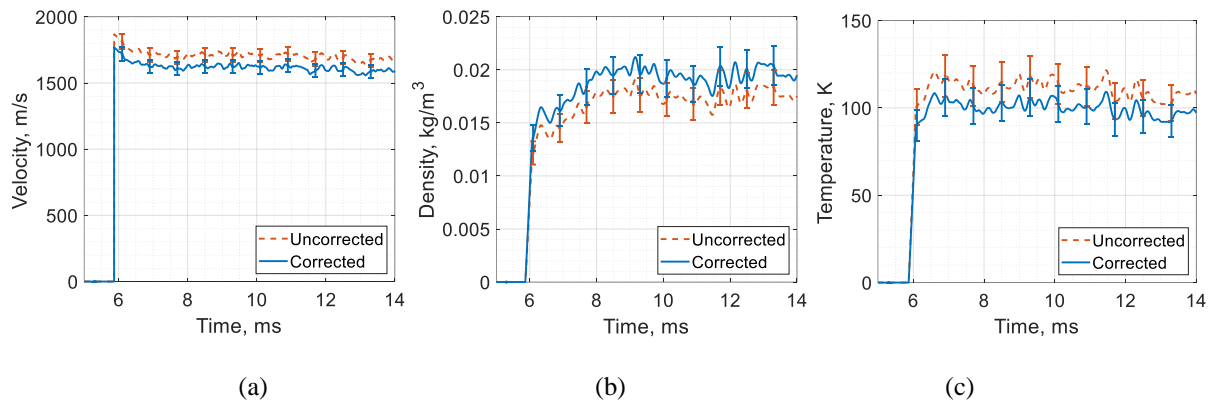

(a)   (b)   (c)

Figure 15.   Freestream (a) velocity, (b) density and (c) temperature for the TH2 condition I obtained using the rebuilding method.

Another aspect of the test conditions which needs to be studied is the thermochemical state of the freestream. From theoretical calculations, the test flow generated is expected to be at an excited thermochemical state which is frozen from some point not far downstream of the throat [67]. Coherent anti-stokes Raman spectroscopy showed that even the test flow from a cold hypersonic facility could have significant vibrational excitation [5, 68]. For the TH2 condition I, differences of around 5 – 10 % between the equilibrium and frozen results for the freestream velocity, temperature and density are observed. The differences increase as the total enthalpy of the test conditions increase. For example, the differences between the frozen and equilibrium freestream properties is around 10 – 20 % for the TH2 condition III as shown in Figure 16.
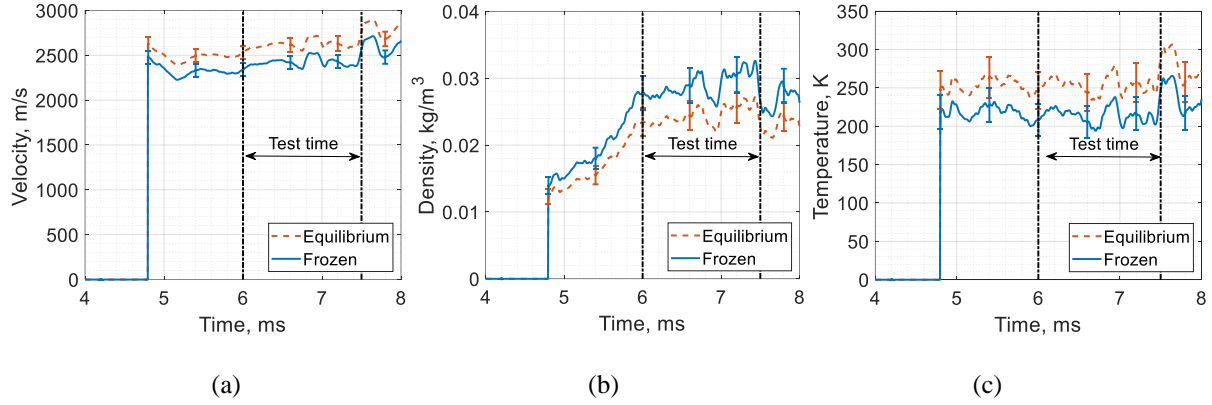
24

Figure 16. Rebuilt freestream (a) velocity, (b) density and (c) temperature of the TH2 condition III.

It is well known that the nozzle exit static pressure, as well as being a good indicator of helium contamination, is also a good indicator of the thermochemical state of the freestream. In the current work, the measured static pressure is compared to that calculated from isentropic quasi-one-dimensional nozzle flow. The isentropic prediction is calculated from the reservoir condition obtained using the measured shock speed and reservoir pressure, and the solution is anchored to the measured nozzle exit pitot pressure. This is done in well-known shock tunnel condition estimating codes such as ESTCj [69] and STN [52]. An example of the result is shown in Figure 17 (b) for condition III; in the indicated test time, the measured static pressure is clearly closer to the frozen limit of the static pressure which is calculated assuming the vibrational and chemical modes freeze at the throat condition. The same is observed for condition IV. This result is consistent with the theory of Ref. [67], and shows that the nonequilibrium flow through the TH2 nozzle for condition III and condition IV behaves as expected, which is not always the case for nozzles of hypersonic facilities. For example, Sagnier and Vérant [70, 71] showed that in the nozzle of the F4 hotshot, the flow was close to thermochemical equilibrium for low and high enthalpy air conditions even though the theory and computation predicted frozen flows. Regarding the TH2 condition I and condition II, the difference between the equilibrium and frozen static pressure is too small to make any inferences, as shown in Figure 17 (a).
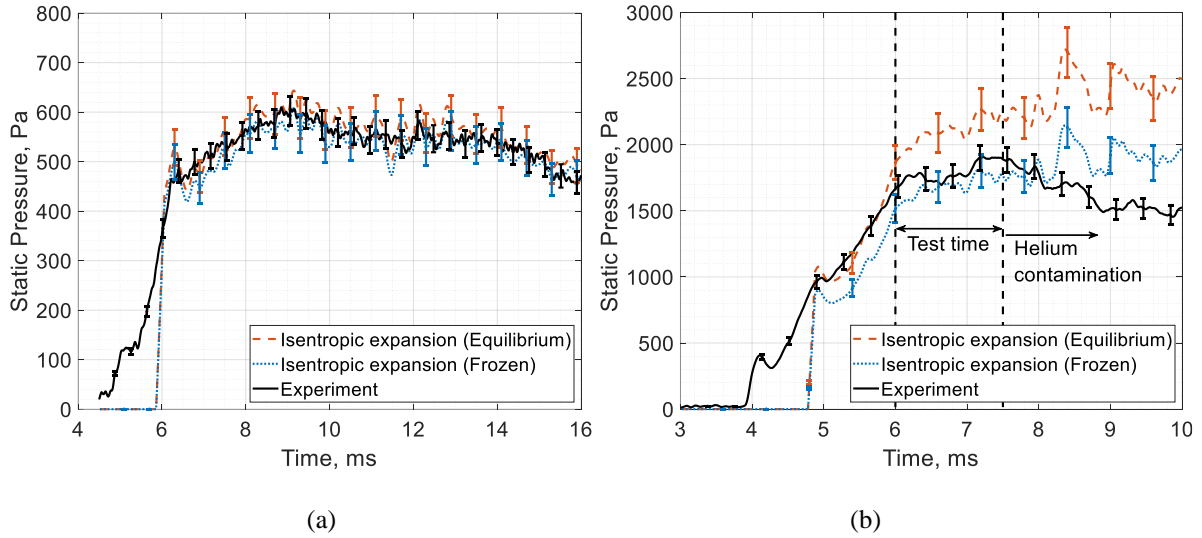
Figure 17. Nozzle exit static pressure measurements compared to the calculated static pressures from pitot pressure anchored isentropic expansions for the TH2 conditions (a) I and (b) III.
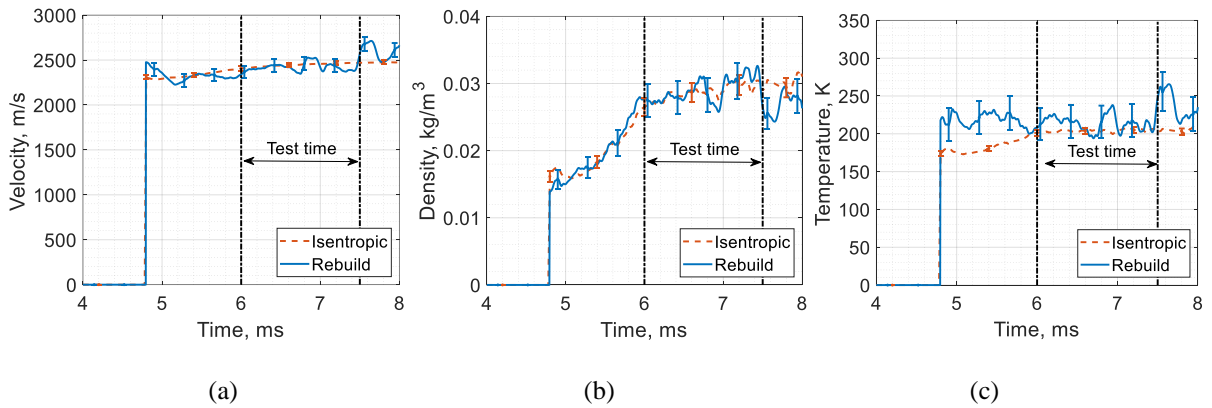

Figure 18. Frozen freestream (a) velocity, (b) density and (c) temperature of the TH2 condition III.

In light of Figure 17 (b), one should take the frozen limit of the freestream estimate from the rebuilding method as the most accurate estimate of the test condition, especially for the TH2 condition III and condition IV. The vibrational temperature and chemical composition in the freestream should be set equal to those at the throat, unless better estimates from thermochemical nonequilibrium nozzle computations using codes such as STUBE (which solves the quasi-one-dimensional steady Euler equations with thermochemical nonequilibrium) [51] can be obtained since freezing occurs shortly downstream of the throat and not exactly at the throat. Having a thermochemically excited test flow is undesirable but, unfortunately, it is often unavoidable. Thermochemical excitation in the freestream could have significant influences on a number of different hypersonic flow phenomena – this is true even in cold hypersonics flows where the chemistry is inactive but the vibrational mode is active. Through numerical simulations, the thermochemical state of the freestream was shown to be important for hypersonic double-cone flows even at low enthalpy pure N_2 conditions of around 3.7 MJ/kg [72]. For blunt body

flows, Stalker [73] gave a rough rule which states that, if the freestream enthalpy is less than a third of the total enthalpy, then effects of freestream non-equilibrium on the real-gas effects in the flow over the body are small. This condition is achieved for all four TH2 conditions even when the frozen limit is assumed, where h_∞/h_0 is no more than 20 %.

Lastly, the current work is related to the work of Ref. [16, 74] who used the original rebuilding technique of Olivier [12] to rebuild the test conditions in the VKI Longshot gun tunnel. By performing the same analysis shown in Figure 17, they discovered that the measured static pressure was around 50 % higher than the equilibrium isentropic expansion result, and lay outside the frozen and equilibrium bounds. They attributed this to a non-isentropic nozzle flow, though an explanation for what caused the non-isentropic flow was not given. This phenomenon is not observed in the current work. Consequently, good agreement is observed between the frozen isentropic quasi-one-dimensional nozzle flow result and the frozen freestream rebuilding result, as shown in Figure 18. This finding further validates the current rebuilding method and shows that the TH2 nozzle flows are almost isentropic. Because thermochemical nonequilibrium flows are non-isentropic [20], the indication of frozen isentropic nozzle flows shown here suggests that the non-equilibrium region near the throat, which must exist as the flow transitions from equilibrium in the converging section to frozen in the diverging section, is small and that the transition from equilibrium to frozen occurs suddenly. This is consistent with the existing theoretical and numerical results [49, 67].

6   On the benefits of the rebuilding method

The rebuilding method outlined in section 2 and exemplified in section 5 has a number of qualitative benefits in addition to the quantitative benefits shown in section 5. Firstly, the method is simple. While it is acknowledged that the need to perform CFD simulations on a sphere to determine the Fay-Riddell correction factors complicates the technique, overall, it is still simpler than some of the other methods. For example, if one is to characterize the test conditions by performing Navier-Stokes simulations of the nozzle, iterations would have to be conducted to tune the defined boundary layer transition location along the nozzle such that the computed pitot pressure distribution at the nozzle exit matches with the corresponding measurement [10]. This is thus a formidable computational task which also requires experimental input in the form of the measured pitot pressure distribution at the nozzle exit. The rebuilding method exchanges this for CFD simulations of a small sphere which is simpler to conduct than that of a large nozzle which requires more computational cells in addition to requiring iterations and pitot pressure distribution measurements. Likewise, if one wants to characterize the test conditions via laser

27

diagnostics, a specialist would have to be hired to do the job due to the complexity of these techniques. It is stressed that the rebuilding method only requires the CFD simulations on a sphere to be performed once for a nominal test condition. After that, an individual freestream estimate can be obtained for each individual run without needing any further computational work.

This leads to the second benefit of the current technique which is that a unique freestream estimate can be obtained for each individual run concurrently with any on-going experiments without interference. This is possible due to 1) the use of small pressure and heat flux probes which can be placed permanently in the test section without occupying significant space in the core flow, and 2) the simplicity of the post-processing procedure which completes in less than 10 minutes on a standard personal computer. This benefit is generally more difficult to achieve when using the other methods (nozzle CFD and laser). While it is acknowledged that the spherical probes will produce a shock whose size grows downstream in the afterbody, possibly reducing the available space for experimental testing of very long slender bodies, the shock should be very weak at such locations very far downstream though. Also, the testing of such a long slender body might be impossible in the first place, irrespective of the presence of the permanent probes, due to the test time limitation of the facility and the converging expansion fan originating at the nozzle exit wall.

Another benefit of the current rebuilding method is that it produces time-resolved results. This is particularly desirable in test facilities with long test times which are quasi-steady. For example, the VKI Longshot gun tunnel benefited from the time-resolution of the results, as demonstrated in Ref. [16], obtained from the original rebuilding technique of Olivier [12] (no Fay-Riddell correction factor). Despite the current work being focused on the reflected shock tunnel, no loss of generality occurs in the derivation of the current rebuilding technique therefore it is applicable in any hypersonic impulse facility including gun tunnels, shock tunnels, and expansion tunnels. Furthermore, no assumptions are made in the current rebuilding method to relate the reservoir condition to the nozzle exit condition, such as assuming the reservoir enthalpy is equal to the nozzle exit total enthalpy or an isentropic nozzle flow. Although these are shown to be valid for the current conditions, this is not always the case in hypersonic impulse facilities as shown in Ref. [16, 66]. No loss of generality is made in the rebuilding methodology which enables the assessment of these assumptions as demonstrated here.

Lastly, and probably most importantly, the current rebuilding method provides an additional independent characterization of the test condition which can be interpreted together with the results from the other methods. Each method has its own benefits. Ultimately, one would want to have many independent estimates of the test conditions for experimenters to make true assessments where freestream conditions are critical. Due to the

simplicity of the current rebuilding method, it can be easily implemented in existing facilities to provide an additional estimate alongside existing results.

7 Conclusion

A new method to characterize hypersonic impulse facilities is introduced. The method is a simple yet accurate hybrid experimental-computational rebuilding method which uses the Fay-Riddell correlation with corrections based on thermochemical nonequilibrium CFD results which are rigorously assessed and validated. Corrections for underpredictions of less than 20 % for the stagnation point heat flux are required via the use of correction factors. These underpredictions are likely caused by deviations of the real tangential velocity gradient from the theoretical one based on Newtonian theory and by the influence of thermochemical nonequilibrium in the flow around the sphere.

The work done characterizing four test conditions in the TH2 reflected shock tunnel is detailed. Particular focus is given to the total enthalpy where a comparison is made with the reservoir enthalpy determined using the measured shock speed and pressure in the shock tube. Better results are obtained in all cases when the correction factor is applied. This justifies the use of the correction factor and provides confidence in the freestream solutions produced from the new method. Additionally, static pressure measurements showed that the TH2 conditions III and IV have a thermochemical state which likely froze shortly after the nozzle throat. Therefore, for these two conditions, it is necessary to take the frozen limit of the rebuilt freestream for postprocessing of experimental data. Furthermore, from the static pressure measurements and the results of the freestream rebuilding, the TH2 nozzle flows are shown to be almost isentropic.

The benefits of the introduced rebuilding method include simplicity and time-resolution, and, using this method, a unique characterization can be made for each individual experimental run. Simplicity is achieved by avoiding the use of any optical techniques and overly expensive numerical computations. The method is applicable and easily implementable in any hypersonic impulse facility including gun tunnels, shock tunnels, and expansion tunnels. It avoids the need to make assumptions to relate the nozzle supply condition to the nozzle exit condition, such as assuming the reservoir enthalpy is equal to the nozzle exit total enthalpy or an isentropic nozzle flow, and it can be easily implemented in existing facilities to provide an additional estimate alongside existing results.

Data Availability Statement

The data that supports the findings of this study are available within the article [and its supplementary material].

References

1.   Olivier, H. "The Aachen shock tunnel TH2 with dual driver mode operation," *Experimental Methods of Shock Wave Research*. Springer, 2016, pp. 111-129.

2.   Reynier, P. "Survey of high-enthalpy shock facilities in the perspective of radiation and chemical kinetics investigations," *Progress in Aerospace Sciences* Vol. 85, 2016, pp. 1-32.
https://doi.org/10.1016/j.paerosci.2016.04.002

3.   Olivier, H., and Gu, S. "Operation, capabilities and limitations of existing hypersonic facilities," *VKI Lecture Series: Flow characterization and modeling of hypersonic wind tunnels*. STO-EN AVT-325-01, von Karman Institute for Fluid Dynamics, Sint-Genesius-Rode, Belgium, 2018.

4.   Girard, J. J., Finch, P. M., Strand, C. L., Hanson, R. K., Yu, W. M., Austin, J. M., and Hornung, H. G. "Measurements of reflected shock tunnel freestream nitric oxide temperatures and partial pressure," *AIAA Journal* Vol. 59, No. 12, 2021, pp. 5266-5275.
https://doi.org/10.2514/1.J060596

5.   Miles, R., Dogariu, A., and Dogariu, L. "Localized time accurate sampling of nonequilibrium and unsteady hypersonic flows: methods and horizons," *Experiments in Fluids* Vol. 62, No. 12, 2021, pp. 1-14.
https://doi.org/10.1007/s00348-021-03332-2

6.   Chandel, D., Nompelis, I., and Candler, G. V. "Numerical Simulations of Shock Propagation Under Strong Nonequilibrium Conditions," *Journal of Thermophysics and Heat Transfer* Vol. 34, No. 3, 2020, pp. 556-569.
https://doi.org/10.2514/1.T5882

7.   Gildfind, D., Jacobs, P., Morgan, R., Chan, W., and Gollan, R. "Scramjet test flow reconstruction for a large-scale expansion tube, Part 2: axisymmetric CFD analysis," *Shock Waves*, 2017, pp. 1-20.
https://doi.org/10.1007/s00193-017-0786-9

8.   McGilvray, M., Dann, A., and Jacobs, P. "Modelling the complete operation of a free-piston shock tunnel for a low enthalpy condition," *Shock waves* Vol. 23, No. 4, 2013, pp. 399-406.
https://doi.org/10.1007/s00193-013-0437-8

9.   Gimelshein, S. F., and Wysong, I. J. "Nonequilibrium effects in high enthalpy gas flows expanding through nozzles," *Physics of Fluids* Vol. 33, No. 10, 2021, p. 106104.
https://doi.org/10.1063/5.0068917

10.   Hannemann, K. "High enthalpy flows in the HEG shock tunnel: experiment and numerical rebuilding," *41st Aerospace Sciences Meeting and Exhibit*. AIAA Paper 2003-978, January 2003.
https://doi.org/10.2514/6.2003-978.

11.   Lee, S., Kim, I., Park, G., Lee, J. K., and Kim, J. G. "Thermochemical nonequilibrium flow analysis in low enthalpy shock-tunnel facility," *PloS one* Vol. 15, No. 10, 2020, p. e0240300.
https://doi.org/10.1371/journal.pone.0240300

12.   Olivier, H. "An improved method to determine free stream conditions in hypersonic facilities," *Shock Waves* Vol. 3, No. 2, 1993, pp. 129-139.
https://doi.org/10.1007/BF02115892

13.   Fay, J. A., and Riddell, F. R. "Theory of stagnation point heat transfer in dissociated air," *Journal of the Aerospace Sciences* Vol. 25, No. 2, 1958, pp. 73-85.
https://doi.org/10.2514/8.7517

14.   Brandis, A. M., and Johnston, C. O. "Characterization of stagnation-point heat flux for earth entry," *45th AIAA Plasmadynamics and Lasers Conference*. AIAA Paper 2014-2374, June 2014
https://doi.org/10.2514/6.2014-2374.

15.   Gu, S., and Olivier, H. "Characterization of a low enthalpy condition generated in a reflected shock tunnel," *32nd International Symposium on Shock Waves*. Springer, Singapore, 2019.

16.   Grossir, G., Dias, B., Chazot, O., and Magin, T. "High temperature and thermal non-equilibrium effects on the determination of free-stream flow properties in hypersonic wind tunnels," *Physics of Fluids* Vol. 30, No. 12, 2018, p. 126102.
https://doi.org/10.1063/1.5058098

17.   Tanno, H., Komuro, T., Lillard, R. P., and Olejniczak, J. "Experimental study of high-enthalpy heat flux augmentation in shock tunnels," *Journal of Thermophysics and Heat Transfer* Vol. 29, No. 4, 2015, pp. 858-862.
https://doi.org/10.2514/1.T4478

18.   Cruden, B. A., Tang, C. Y., Olejniczak, J., Amar, A. J., and Tanno, H. "Characterization of radiative heating anomaly in high enthalpy shock tunnels," *Experiments in Fluids* Vol. 62, No. 7, 2021, pp. 1-17.
https://doi.org/10.1007/s00348-021-03227-2

19.   Kindl, H., Olivier, H., Zhao, H., Muylaert, J., Wong, H., and Walpot, L. "Conventional flow diagnostics in shock tunnels," *Proceedings 21st International Symposium on Shock Waves*. Great Keppel Island, Australia, 1997, pp. 493-498.

20.   Anderson, J. D. *Modern compressible flow: with historical perspective*. New York: McGraw-Hill New York, 2021.

21.   Goodwin, D. G., Speth, R. L., Moffat, H. K., and Weber, B. W. *Cantera: An object-oriented software toolkit for chemical kinetics, thermodynamics, and transport processes*. https://www.cantera.org, 2021. Version 2.5.1.
doi:10.5281/zenodo.4527812

22.   Gollan, R. J., and Jacobs, P. A. "About the formulation, verification and validation of the hypersonic flow solver Eilmer," *International Journal for Numerical Methods in Fluids* Vol. 73, No. 1, 2013, pp. 19-57.
https://doi.org/10.1002/fld.3790

23.   Park, G., Gai, S. L., and Neely, A. J. "Base flow of circular cylinder at hypersonic speeds," *AIAA Journal* Vol. 54, No. 2, 2016, pp. 458-468.
https://doi.org/10.2514/1.J054270

24.   Deepak, N., Gai, S., and Neely, A. "High-enthalpy flow over a rearward-facing step–a computational study," *Journal of Fluid Mechanics* Vol. 695, 2012, pp. 405-438.
https://doi.org/10.1017/jfm.2012.29

25.   Ewenz Rocher, M., Hermann, T., McGilvray, M., and Gollan, R. "Correlation for Species Concentration on a Hypersonic Stagnation Point with Mass Injection," *AIAA Journal*, 2021, pp. 1-12.
https://doi.org/10.2514/1.J061159

26.   Yang, Y., and Park, G. "Analysis of catalytic heat transfer for a multi-species gas mixture," *International Journal of Heat and Mass Transfer* Vol. 137, 2019, pp. 1088-1102.
https://doi.org/10.1016/j.ijheatmasstransfer.2019.03.172

27.   Macrossan, M. "The equilibrium flux method for the calculation of flows with non-equilibrium chemical reactions," *Journal of Computational Physics* Vol. 80, No. 1, 1989, pp. 204-231.
https://doi.org/10.1016/0021-9991(89)90095-8

28.   Wada, Y., and Liou, M.-S. "A flux splitting scheme with high-resolution and robustness for discontinuities," *32nd Aerospace Sciences Meeting and Exhibit*. AIAA Paper 1994-83, January, 1994.
https://doi.org/10.2514/6.1994-83.

29. Van Albada, G. D., Leer, B. v., and Roberts, W. "A comparative study of computational methods in cosmic gas dynamics," *Upwind and high-resolution schemes*. Springer, Berlin, Heidelberg, 1997, pp. 95-103.

30. Van Leer, B. "Towards the ultimate conservative difference scheme. V. A second-order sequel to Godunov's method," *Journal of Computational Physics* Vol. 32, No. 1, 1979, pp. 101-136. https://doi.org/10.1016/0021-9991(79)90145-1

31. Oran, E. S., and Boris, J. P. *Numerical simulation of reactive flow*. Cambridge: Cambridge university press, 2001.

32. Ramshaw, J., and Chang, C. "Computational fluid dynamics modeling of multicomponent thermal plasmas," *Plasma Chemistry and Plasma Processing* Vol. 12, No. 3, 1992, pp. 299-325. https://doi.org/10.1007/BF01447028

33. Gupta, R. N., Yos, J. M., Thompson, R. A., and Lee, K.-P. "A review of reaction rates and thermodynamic and transport properties for an 11-species air model for chemical and thermal nonequilibrium calculations to 30000 K." Langley Research Center NASA STI/Recon Technical Report NASA-RP-1232, Hampton, VA., 1990.

34. Jacobs, P., Gollan, R., Denman, A., O'Flaherty, B., Potter, D., Petrie-Repar, P., and Johnston, I. "Eilmer's theory book: basic models for gas dynamics and thermochemistry." Department of Mechanical Engineering Report 2010/09, The University of Queensland, 2010.

35. Park, C. "Review of chemical-kinetic problems of future NASA missions. I-Earth entries," *Journal of Thermophysics and Heat transfer* Vol. 7, No. 3, 1993, pp. 385-398. https://doi.org/10.2514/3.431

36. Papadopoulos, P., Venkatapathy, E., Prabhu, D., Loomis, M. P., and Olynick, D. "Current grid-generation strategies and future requirements in hypersonic vehicle design, analysis and testing," *Applied Mathematical Modelling* Vol. 23, No. 9, 1999, pp. 705-735. https://doi.org/10.1016/S0307-904X(99)00007-4

37. Ren, X., Yuan, J., He, B., Zhang, M., and Cai, G. "Grid criteria for numerical simulation of hypersonic aerothermodynamics in transition regime," *Journal of Fluid Mechanics* Vol. 881, 2019, pp. 585-601. https://doi.org/10.1017/jfm.2019.756

38. Liu, C., Zhou, G., Shyy, W., and Xu, K. "Limitation principle for computational fluid dynamics," *Shock Waves* Vol. 29, No. 8, 2019, pp. 1083-1102. https://doi.org/10.1007/s00193-018-0881-6

39. Murzinov, I. N. "Laminar boundary layer on a sphere in hypersonic flow of equilibrium dissociating air," *Fluid Dynamics* Vol. 1, No. 2, 1966, pp. 131-133. https://doi.org/10.1007/BF01013841

40. Lees, L. "Laminar heat transfer over blunt-nosed bodies at hypersonic flight speeds," *Journal of Jet Propulsion* Vol. 26, No. 4, 1956, pp. 259-269. https://doi.org/10.2514/8.6977

41. Roache, P. J. "Quantification of uncertainty in computational fluid dynamics," *Annual Review of Fluid Mechanics* Vol. 29, No. 1, 1997, pp. 123-160. https://doi.org/10.1146/annurev.fluid.29.1.123

42. Fujiwara, Y., Tezuka, A., Shimamura, K., Okamoto, T., Yamada, K., Komuro, T., Tanno, H. "Measurement of stagnation heat flux in HEK-X expansion tube," *32nd International Symposium on Shock Waves*. Springer, Singapore, 2019.

43. Olivier, H. "Influence of the velocity gradient on the stagnation point heating in hypersonic flow," *Shock Waves* Vol. 5, No. 4, 1995, pp. 205-216. https://doi.org/10.1007/BF01419002

44. Ilich, Z., Grossir, G., and Chazot, O. "Evaluation of the stagnation-point velocity gradient in low-enthalpy hypersonic flows," *33rd AIAA Aerodynamic Measurement Technology and Ground Testing Conference*. AIAA Paper 2017-3984, June 2017 https://doi.org/10.2514/6.2017-3984.

45. Gokcen, T. "Effects of freestream nonequilibrium on convective heat transfer to a blunt body," *Journal of Thermophysics and Heat Transfer* Vol. 10, No. 2, 1996, pp. 234-241. https://doi.org/10.2514/3.780

46. Candler, G. V. "Rate effects in hypersonic flows," *Annual Review of Fluid Mechanics* Vol. 51, 2019, pp. 379-402. https://doi.org/10.1146/annurev-fluid-010518-040258

47. Tchuen, G., and Zeitoun, D. E. "Effects of chemistry in nonequilibrium hypersonic flow around blunt bodies," *Journal of Thermophysics and Heat Transfer* Vol. 23, No. 3, 2009, pp. 433-442. https://doi.org/10.2514/1.42665

48. Park, C. "Thermochemical relaxation in shock tunnels," *Journal of Thermophysics and Heat Transfer* Vol. 20, No. 4, 2006, pp. 689-698. https://doi.org/10.2514/1.22719

49. Hall, J. G., and Treanor, C. E. "Nonequilibrium effects in supersonic-nozzle flows." AGARDograph No. 124, 1967.

50. McIntosh, M. "Computer program for the numerical calculation of frozen and equilibrium conditions in shock tunnels." Dept. of Physics, Internal Rept., Australian National Univ., Canberra, Australia, 1968.

51. Vardavas, I. "Modelling reactive gas flows within shock tunnels," *Australian Journal of Physics* Vol. 37, No. 2, 1984, pp. 157-178. https://doi.org/10.1071/PH840157

52. Krek, R. M., and Jacobs, P. A. "STN, shock tube and nozzle calculations for equilibrium air." Rep. 2/93. Department of Mechanical Engineering, University of Queensland, 1993.

53. Jacobs, P. "Quasi-one-dimensional modeling of a free-piston shock tunnel," *AIAA Journal* Vol. 32, No. 1, 1994, pp. 137-145. https://doi.org/10.2514/3.11961

54. Jacobs, P. A. "Approximate Riemann solver for hypervelocity flows," *AIAA Journal* Vol. 30, No. 10, 1992, pp. 2558-2561. https://doi.org/10.2514/3.11264

55. McBride, B. J., and Gordon, S. "Computer program for calculation of complex chemical equilibrium compositions and applications. II. Users manual and program description." NASA Reference Publication 1311, 1996.

56. Groth, C. P., Gottlieb, J., and Sullivan, P. "Numerical investigation of high-temperature effects in the UTIAS–RPI hypersonic impulse tunnel," *Canadian Journal of Physics* Vol. 69, No. 7, 1991, pp. 897-918. https://doi.org/10.1139/p91-144

57. Mundt, C., Boyce, R., Jacobs, P., and Hannemann, K. "Validation study of numerical simulations by comparison to measurements in piston-driven shock-tunnels," *Aerospace Science and Technology* Vol. 11, No. 2-3, 2007, pp. 100-109. https://doi.org/10.1016/j.ast.2006.12.002

58. Gildfind, D., Jacobs, P., Morgan, R., Chan, W., and Gollan, R. "Scramjet test flow reconstruction for a large-scale expansion tube, Part 1: quasi-one-dimensional modelling," *Shock Waves*, 2017, pp. 1-21. https://doi.org/10.1007/s00193-017-0785-x

59. Grossir, G., Ilich, Z., and Chazot, O. "Modeling of the VKI Longshot gun tunnel compression process using a quasi-1D approach," *33rd AIAA Aerodynamic Measurement Technology and Ground Testing Conference*. AIAA Paper 2017-3985, June 2017
https://doi.org/10.2514/6.2017-3985.

60. Collen, P., Doherty, L. J., Subiah, S. D., Sopek, T., Jahn, I., Gildfind, D., Penty Geraets, R., Gollan, R., Hambidge, C., and Morgan, R. "Development and commissioning of the T6 Stalker Tunnel," *Experiments in Fluids* Vol. 62, No. 11, 2021, pp. 1-24.
https://doi.org/10.1007/s00348-021-03298-1

61. Mee, D. J. "Uncertainty analysis of conditions in the test section of the T4 shock tunnel." Department of Mechanical Engineering Report 4/93, The University of Queensland, 1993.

62. Jewell, J. S. "Boundary-layer transition on a slender cone in hypervelocity flow with real gas effects." Ph.D. Dissertation, California Institute of Technology, Pasadena, CA, 2014.

63. Thiele, T., Gülhan, A., and Olivier, H. "Instrumentation and aerothermal postflight analysis of the rocket technology flight experiment ROTEX-T," *Journal of Spacecraft and Rockets* Vol. 55, No. 5, 2018, pp. 1050-1073.
https://doi.org/10.2514/1.A34129

64. Grossir, G., Van Hove, B., Paris, S., Rambaud, P., and Chazot, O. "Free-stream static pressure measurements in the Longshot hypersonic wind tunnel and sensitivity analysis," *Experiments in Fluids* Vol. 57, No. 5, 2016, p. 64.
https://doi.org/10.1007/s00348-016-2137-5

65. Jiang, H., Liu, J., Luo, S., Huang, W., Wang, J., and Liu, M. "Thermochemical non-equilibrium effects on hypersonic shock wave/turbulent boundary-layer interaction," *Acta Astronautica* Vol. 192, 2022, pp. 1-14.
https://doi.org/10.1016/j.actaastro.2021.12.010

66. Logan, P., Stalker, R., and McIntosh, M. "A shock tube study of radiative energy loss from an argon plasma," *Journal of Physics D: Applied Physics* Vol. 10, No. 3, 1977, p. 323.
https://doi.org/10.1088/0022-3727/10/3/012

67. Bray, K. N. C. "Atomic recombination in a hypersonic wind-tunnel nozzle," *Journal of Fluid Mechanics* Vol. 6, No. 1, 1959, pp. 1-32.
https://doi.org/10.1017/S0022112059000477

68. Cutler, A. D., Cantu, L. M., Gallo, E. C., Baurle, R., Danehy, P. M., Rockwell, R., Goyne, C., and McDaniel, J. "Nonequilibrium supersonic freestream studied using coherent anti-Stokes Raman spectroscopy," *AIAA Journal* Vol. 53, No. 9, 2015, pp. 2762-2770.
https://doi.org/10.2514/1.J053748

69. Jacobs, P., Gollan, R., Potter, D., Zander, F., Gildfind, D., Blyton, P., Chan, W., and Doherty, L. "Estimation of high-enthalpy flow conditions for simple shock and expansion processes using the ESTCj program and library." Mechanical Engineering Report 2011/02, Department of Mechanical Engineering, University of Queensland, Australia, 2014.

70. Sagnier, P., and Verant, J.-L. "Flow characterization in the ONERA F4 high-enthalpy wind tunnel," *AIAA Journal* Vol. 36, No. 4, 1998, pp. 522-531.
https://doi.org/10.2514/2.425

71. Sagnier, P., and Vérant, J.-L. "On the validation of high enthalpy wind tunnel simulations," *Aerospace Science and Technology* Vol. 2, No. 7, 1998, pp. 425-437.
https://doi.org/10.1016/S1270-9638(99)80002-9

72. Nompelis, I., Candler, G. V., and Holden, M. S. "Effect of vibrational nonequilibrium on hypersonic double-cone experiments," *AIAA Journal* Vol. 41, No. 11, 2003, pp. 2162-2169.

https://doi.org/10.2514/2.6834

73. Stalker, R. "Hypervelocity aerodynamics with chemical nonequilibrium," *Annual Review of Fluid Mechanics* Vol. 21, No. 1, 1989, pp. 37-60.
https://doi.org/10.1146/annurev.fl.21.010189.000345

74. Khraibut, A., Chazot, O., Magin, T., and Gai, S. "A numerical study of thermal nonequilibrium and high-density effects on the VKI Longshot contoured nozzle," *AIAA Scitech 2021 Forum*. AIAA Paper 2021-0493, January 2021.
https://doi.org/10.2514/6.2021-0493.